NANO LETTERS

Letter

pubs.acs.org/NanoLett

Out-of-Plane Electromechanical Response of Monolayer Molybdenum Disulfide Measured by Piezoresponse Force Microscopy

Christopher J. Brennan,[†,‡] Rudresh Ghosh,[†,‡] Kalhan Koul,[†,‡] Sanjay K. Banerjee,[†,‡,§] Nanshu Lu,[*,†,‡,§,∥,⊥] and Edward T. Yu[*,†,‡,§]

[†]Microelectronics Research Center, University of Texas at Austin, Austin, Texas 78758, United States

[‡]Department of Electrical and Computer Engineering, University of Texas at Austin, Austin, Texas 78701, United States

[§]Texas Materials Institute, University of Texas at Austin, Austin, Texas 78712, United States

[∥]Center for Mechanics of Solids, Structures, and Materials, Department of Aerospace Engineering and Engineering Mechanics, University of Texas at Austin, Austin, Texas 78712, United States

[⊥]Department of Biomedical Engineering, University of Texas at Austin, Austin, Texas 78712, United States

Supporting Information

ABSTRACT: Two-dimensional (2D) materials have recently been theoretically predicted and experimentally confirmed to exhibit electromechanical coupling. Specifically, monolayer and few-layer molybdenum disulfide (MoS_2) have been measured to be piezoelectric within the plane of their atoms. This work demonstrates and quantifies a nonzero out-of-plane electromechanical response of monolayer MoS_2 and discusses its possible origins. A piezoresponse force microscope was used to measure the out-of-plane deformation of monolayer MoS_2 on Au/Si and Al_2O_3/Si substrates. Using a vectorial background subtraction technique, we estimate the effective out-of-plane piezoelectric coefficient, d_{33}^{eff}, for monolayer MoS_2 to be 1.03 ± 0.22 pm/V when measured on the Au/Si substrate and 1.35 ± 0.24 pm/V when measured on Al_2O_3/Si. This is on the same order as the in-plane coefficient d_{11} reported for monolayer MoS_2. Interpreting the out-of-plane response as a flexoelectric response, the effective flexoelectric coefficient, μ_{eff}^{*}, is estimated to be 0.10 nC/m. Analysis has ruled out the possibility of elastic and electrostatic forces contributing to the measured electromechanical response. X-ray photoelectron spectroscopy detected some contaminants on both MoS_2 and its substrate, but the background subtraction technique is expected to remove major contributions from the unwanted contaminants. These measurements provide evidence that monolayer MoS_2 exhibits an out-of-plane electromechanical response and our analysis offers estimates of the effective piezoelectric and flexoelectric coefficients.

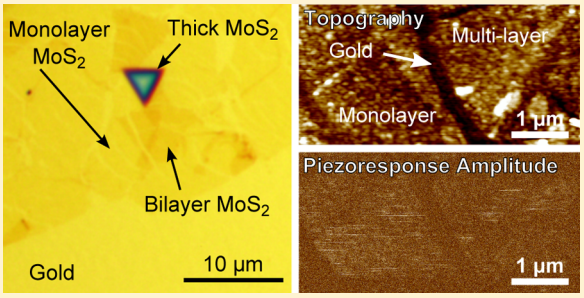

KEYWORDS: *MoS_2, electromechanical coupling, flexoelectricity, piezoelectricity, piezoresponse force microscopy*

The coupling of electronic and mechanical behaviors in crystalline materials has created many engineering opportunities. Strain is commonly used in electronics to alter electronic bandgaps and carrier mobilities,[1] and electromechanical coupling is widely used in microelectromechanical systems (MEMS) to make sensors,[2] actuators,[3] and generators.[4] One of the most widely used electromechanical coupling phenomena is piezoelectricity, which links crystal polarization and mechanical strain. Piezoelectricity only exists in noncentrosymmetric crystalline materials, limiting the range of possible materials to use for such applications. As scaling trends continue to shrink the feature size of materials, a need arises for nanoscale piezoelectric materials. Two-dimensional (2D) materials are very popular candidates for nanodevices because of their exotic electronic properties,[5] transparency,[6,7] and mechanical robustness,[8] and have recently be shown to be candidates for electromechanical nanotransducers.[9,10]

In the atomically thin limit, transition metal dichalcogenides (TMDs) are intrinsically piezoelectric due to the lack of inversion symmetry in their crystal structure.[11] Piezoelectricity arises within the plane of their atoms and both direct[9,12] and converse[12,13] piezoelectric effects have been experimentally confirmed in monolayer and few layer molybdenum disulfide (MoS_2). In-plane piezoelectricity should only exist in odd-number layers of TMDs where there is no inversion symmetry present and decrease rapidly as the number of layers increases due to cancellation of the responses from oppositely oriented layers.[9] Any strain or electric field applied perpendicular to the surface of the MoS_2 will theoretically yield zero piezoelectric response due to its crystal symmetry.

Received: May 19, 2017
Revised: July 25, 2017
Published: August 1, 2017

DOI: 10.1021/acs.nanolett.7b02123
Nano Lett. 2017, 17, 5464−5471

Piezoelectricity is, however, only one type of electromechanical response possible in crystal lattices. In flexoelectricity, polarization arises from strain gradients as opposed to uniform strain.[14−16] Thus, a fourth-order tensor describes flexoelectricity, while a third-order tensor describes piezoelectricity. With an even-rank tensor, flexoelectricity is present in every crystal class. Despite this, flexoelectricity has been seldom studied because the strain gradients necessary to cause a noticeable change in polarization in macro-scale materials requires very large strains that can fracture the material. However, in nanoscale materials even small strain can cause large gradients to form.

Investigations of flexoelectricity in 2D materials[16−18] have mainly focused on either carbon systems[19−21] or hexagonal boron nitride.[22,23] These works were performed from the modeling side but since 2D materials are the ultimate nanoscale material and can have large strain gradients they can offer a platform for experimental studies of flexoelectricity.

Another reason for the lack of experimental study of flexoelectricity is because piezoelectricity and flexoelectricity are difficult to isolate from each other. We propose a solution to this problem by utilizing the symmetry of MoS_2 and other TMDs. Their crystal class, D_{3h} ($\bar{6}m2$), results in a flexoelectric tensor that has nonzero coefficients in the out-of-plane direction,[24] whereas all out-of-plane piezoelectric coefficients are zero.[11] Flexoelectricity in 2D materials can therefore be studied experimentally if an out-of-plane electromechanical response in MoS_2 is measurable. There have been a few notable experimental studies investigating out-of-plane electromechanical properties of 2D materials, namely on graphene-nitride nanosheets with nonsymmetric holes[25] and graphene forming bonds to the underlying SiO_2 substrate.[26] Neither study suggested an estimate for a flexoelectric coefficient. Interestingly, because 2D materials are essentially only a surface, it becomes ambiguous whether out-of-plane electromechanical effects caused by spatial gradients should be referred to as flexoelectricity or surface piezoelectricity.[14,15] Nevertheless, it is referred to as a flexoelectric response here.

Piezoresponse force microscope (PFM) is used to measure out-of-plane electromechanical deformation resulting from an applied out-of-plane electric field. Because an electric field is inducing a strain, this is referred to as the converse piezoelectric effect; the direct piezoelectric effect is a strain inducing a polarization. In the measurement, an atomic force microscope (AFM) with a conductive probe is used to apply an electric field through the test material by applying a drive voltage, V_d, between the tip and substrate. If there is electromechanical coupling in the material, the AFM tip will be deflected by the expansion and contraction of the material. A lock-in amplifier is used to measure both the amplitude and phase of the response while simultaneously measuring surface topography. (See Figure S1 in the Supporting Information for details regarding the PFM measurement and tip−sample geometry.)

The quantity usually obtained from PFM experiments, d_{33}, is the piezoelectric coefficient that represents the out-of-plane piezoelectric response created by an out-of-plane electric field (see Supporting Information Note 1 for details on calculating d_{33} from PFM signals). In actual PFM experiments, the measurement should be referred to as an effective value, d_{33}^{eff}, because of additional possible contributions to the signal including material clamping,[27] inhomogeneous field effects,[28] and other electromechanical effects. Other factors that may affect the measurement and introduce experimental uncertainty include electrostatic effects,[29] topographic artifacts,[30] cantilever dynamics,[31,32] and instrumental noise.[32]

To help minimize the contribution of nonelectromechanical effects and obtain a quantitative estimate of the true electromechanical response of the test material, a vectorial background subtraction technique is used.[33,34] PFM measurements taken on nonpiezoelectric substrates or without applying V_d serve as two different measurements of the background contribution to the measured MoS_2 signal. These measurements, which have an amplitude and phase component, can then be made into vectors. Next, by performing a vector subtraction of the background signal from the MoS_2 signal, a more accurate representation of d_{33}^{eff} can be obtained. The details of this process will be illustrated with data later in this paper.

Samples are made by transferring CVD grown MoS_2 from a growth substrate to either 70 nm gold (Au) or 5.3 nm alumina (Al_2O_3) deposited on an n^{++} silicon substrate. Detailed sample preparation steps are described in the Methods as well as Figure S2. The Au is used to concentrate the electric field within the MoS_2 and serves as the bottom electrode. The Al_2O_3 serves as a dielectric layer to limit current flow with the n^{++} Si substrate now acting as the bottom electrode. Figure 1 shows a schematic

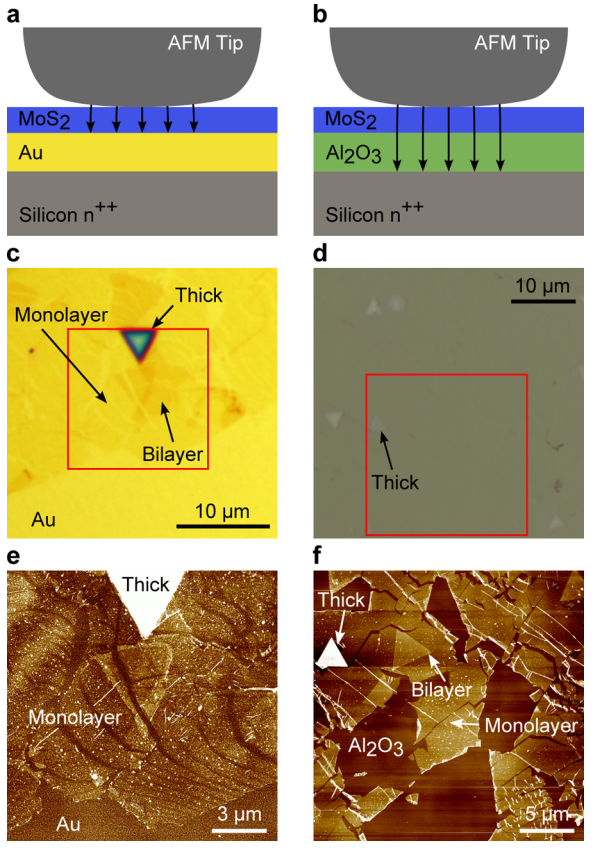

Figure 1. Schematics of the two samples: (a) MoS_2 on 70 nm Au on n^{++} Si and (b) MoS_2 on 5.3 nm Al_2O_3 on n^{++} Si. The black arrows indicate the electric field coming from the AFM tip terminating at the conductive substrates. Because the MoS_2 is monolayer, the AFM tip radius will appear broad in comparison. Optical images of the MoS_2/Au/Si sample (c) and MoS_2/Al_2O_3/Si sample (d) show that the MoS_2 is optically visible on Au but not on the Al_2O_3/Si substrate. Tapping mode AFM images of the MoS_2/Au/Si sample (e) and the MoS_2/Al_2O_3/Si sample (f) show that the monolayer and multilayer MoS_2 layers can be clearly distinguished from the substrate.

DOI: 10.1021/acs.nanolett.7b02123
Nano Lett. 2017, 17, 5464−5471

of the two sample types, along with optical and tapping-mode AFM images of each. The Al_2O_3/Si sample has very limited optical contrast, resulting in very weak Raman and photoluminescence (PL) signals.[35] In this case, tapping-mode AFM was used to identify locations of MoS_2. Figure 2 shows Raman data taken at different locations on each sample. On the Au sample (Figure 2a), the separation of the E^1_{2g} and A_{1g} peaks for MoS_2 increases from 19.7 to 25.7 cm^{-1} from monolayer to thick MoS_2, and both peaks increase in intensity, which is consistent with observations reported in the literature.[36] Only the thick MoS_2 yields measurable Raman data on the Al_2O_3/Si sample (Figure 2b) with a peak separation of 26.1 cm^{-1}. The peak near 520 cm^{-1} is from the underlying silicon. Further discussion of MoS_2 thickness and weak Raman and PL data is provided in Supporting Information Note 2 and Figures S3–S5. PL and Raman measurements at different steps of sample preparation are shown in Figure S6, revealing that residual tensile strain caused during growth is released during the transfer process.

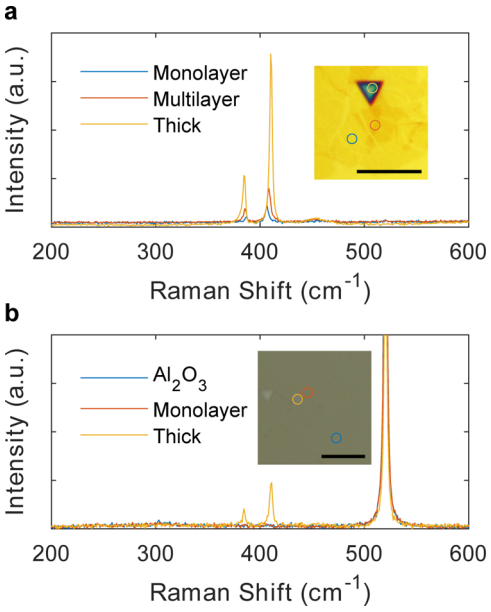

Figure 2. Raman measurements of (a) MoS_2/Au/Si and (b) MoS_2/Al_2O_3/Si samples. The areas measured are circled in the inset microscope images with corresponding colors. The scale bars are 10 μm. The intensity of the MoS_2 Raman signals increases as thicker layers are measured. The peak separation also increases as the thickness increases, as expected. Only the thick MoS_2 region on the Al_2O_3 sample gives a detectable Raman signature due to poor optical absorption caused by the substrate.

Figure 3 shows PFM images of MoS_2 on Au. The topographic (Figure 3a), piezoresponse (PR) amplitude (Figure 3b), and PR phase (Figure 3c) channels with V_d applied show that there is clear contrast between the MoS_2 and the Au. When the voltage is not applied, contrast in topography remains (Figure 3d) whereas contrast in piezoresponse disappears (Figure 3e,f), allowing topographic artifacts to be ruled out.

By using the values measured on Au and those measured without the voltage applied as two separate background signals in the vectorial background subtraction process, we obtain the out-of-plane effective piezoelectric coefficient of MoS_2. As illustrated in Figure 4, with the amplitude and phase information, the measured PR of MoS_2 on Au (black) and the measured PR of the Au background (red) are plotted as two vectors in a 2D x–y graph. In both cases, an average of the amplitude and phase data taken over an area of only monolayer MoS_2 or the Au substrate is done to obtain the two vectors. The difference between the two vectors (blue) is taken to be the true PR coming from the MoS_2. More details of the vectorial background subtraction method can be found in Supporting Information Note 3. The background-subtracted PR can then be converted to a d^{eff}_{33} value using the deflection sensitivity of the cantilever and the drive voltage (details given in Supporting Information Note 1). We finally obtain 0.93 ± 0.23 and 1.12 ± 0.20 pm/V for d^{eff}_{33} of MoS_2 using the Au and the voltage-off condition as the background, respectively. The two values are consistent within our experimental uncertainty, reinforcing that there are minimal topographic artifacts, that the Au makes little to no contribution to the PR, and that the PR is truly associated with the presence of the MoS_2. Detailed analysis of the uncertainty is given in Supporting Information Note 4. In comparison, a piezoelectric lithium niobate ($LiNbO_3$) reference sample has a d_{33} of 7.5 pm/V, d_{11} for

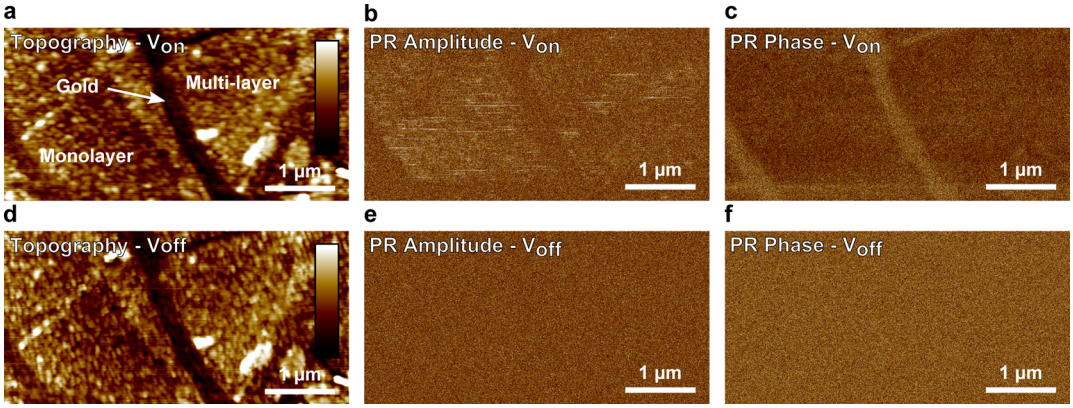

Figure 3. A series of two PFM measurements on the MoS_2/Au sample with the drive voltage applied (V_{on}) (a–c) and not applied (V_{off}) (d–f). The topography images (a,d) show the background Au substrate, monolayer MoS_2, and multilayer MoS_2 regions. The applied drive voltage does not affect the topographic measurement (color bar is 0–5 nm for both). The piezoresonse (PR) amplitude images (b,e) show that the MoS_2 region has contrast against the Au substrate only when the drive voltage is applied (b). The same is true for the PR phase images (c,f). Both amplitude images and phase images share the same color scale.

DOI: 10.1021/acs.nanolett.7b02123
Nano Lett. 2017, 17, 5464–5471

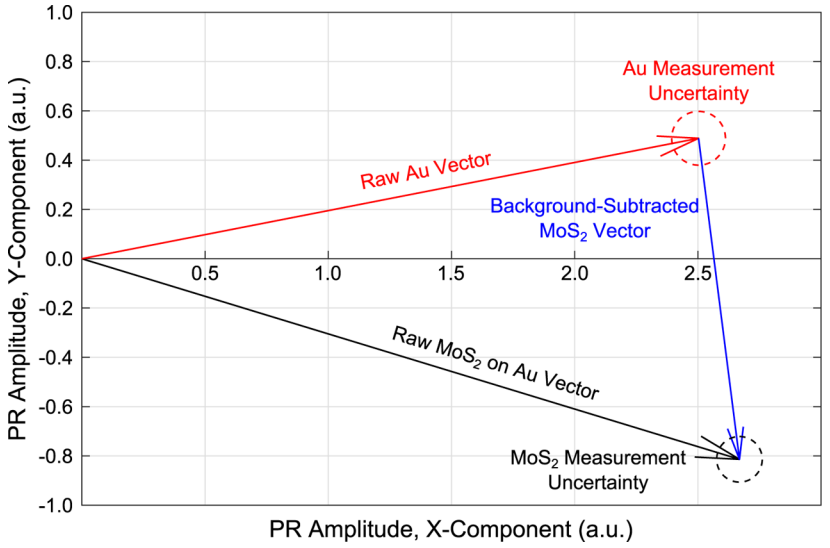

Figure 4. A schematic illustration of how the background subtraction method is performed to calculate d_{33}^{eff}. The amplitude and phase channels of the MoS2 (black) and Au (red) PFM measurements are used to make two separate vectors. The actual signal is the difference between these two vectors (blue). The dashed circles at the end of the vectors represent the uncertainty of the measured amplitudes and phases.

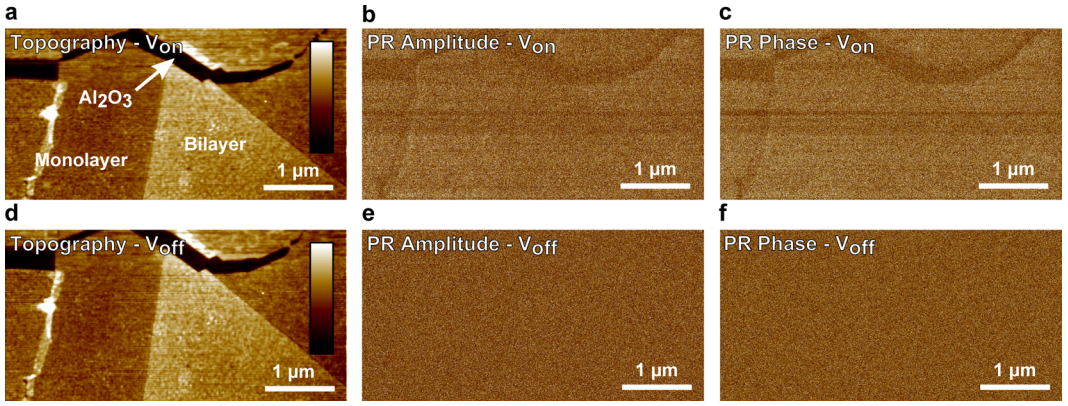

Figure 5. A series of two PFM measurements on the MoS_2/Al_2O_3 sample with the drive voltage applied (V_{on}) (a,b) and not applied (V_{off}) (d–f). The topography images (a,d) show the background Al_2O_3 substrate, monolayer MoS_2, and bilayer MoS_2 regions. The applied drive voltage does not affect the topographic measurement (color bar is 0 to 3.7 nm for both). The PR amplitude images (b,e) show that the MoS_2 region has contrast against the Al_2O_3 substrate only when the drive voltage is applied (b). The same is true for the PR phase images (c,f). Both amplitude images and phase images share the same color scale.

monolayer MoS_2 has been measured[13] to be 1.85 pm/V, and theoretical estimates for d_{11} of MoS_2 range from 2.91 to 3.73 pm/V for clamped- and relaxed-ion cases.[11]

To eliminate the possibility that the observed PR signals are affected by current flow at the tip-MoS_2–Au junction, the Al_2O_3/Si samples were fabricated to limit the potential current flow by introducing an insulating dielectric layer. Figure 5 shows the topographic (Figure 5a), PR amplitude (Figure 5b), and PR phase (Figure 5c) channels of the Al_2O_3/Si sample while V_d is applied. Similar to the case of the Au sample, there are clear differences in the PFM signal on the MoS_2 versus Al_2O_3 when the voltage is applied, but no differences when the voltage is not applied (Figure 5d–f). In this case, an added complication arises because the voltage is being dropped over a larger distance and over two different materials. Given V_d applied between the AFM tip and the n^{++} silicon substrate, the voltage drop across only the MoS_2, V_{MoS_2}, can be estimated using a simple planar capacitance model

$$V_{MoS_2} = V_d \frac{\frac{\epsilon_{Al_2O_3}}{t_{Al_2O_3}}}{\frac{\epsilon_{MoS_2}}{t_{MoS_2}} + \frac{\epsilon_{Al_2O_3}}{t_{Al_2O_3}}} \quad (1)$$

where $\epsilon_{Al_2O_3}$, ϵ_{MoS_2}, $t_{Al_2O_3}$, and t_{MoS_2} are the permittivity of the Al_2O_3 and MoS_2, and the thickness of the Al_2O_3 and MoS_2, respectively (see Supporting Information Note 5). On the basis of the estimated voltage drop, d_{33}^{eff} is calculated to be 1.34 ± 0.27 and 1.35 ± 0.20 pm/V using the Al_2O_3 or the voltage-off condition as the background, respectively. These values are slightly larger than the values measured on Au but are still within our experimental uncertainty. Discrepancies could be caused by variability in the separate AFM tips used, variable wear of the AFM tips, changes caused by the presence or absence of current flow, depletion of carriers in the n^{++} Si bottom electrode, or differences in geometries between the two systems. The results for the two different types of samples are summarized in Table 1. The last column compares the signal

DOI: 10.1021/acs.nanolett.7b02123
Nano Lett. 2017, 17, 5464–5471

measured on the respective substrates to the voltage-off condition, showing that the substrates are not piezoelectric.

Table 1. d_{33}^{eff} and Uncertainty Values Calculated from Preforming Background Subtraction with the Indicated PFM Vectors

	MoS_2 versus Sub (pm/V)	MoS_2 versus V_{off} (pm/V)	Sub versus V_{off} (pm/V)
Au/Si sample	0.93 ± 0.23	1.12 ± 0.20	0.19 ± 0.10
Al_2O_3/Si sample	1.34 ± 0.27	1.35 ± 0.20	0.04 ± 0.15

To understand the origin of the measured d_{33}^{eff} signal in the PFM experiment, including the potential contribution of flexoelectric response, a closer look at the forces involved in the measurement is required. The multiple contributions to the force that acts on the AFM tip can be summarized by

$$F_{tot} = F_0 + F_{ES} + F_{EM} \tag{2}$$

where F_{tot} is the total force, F_0 the elastic force, F_{ES} the electrostatic force, and F_{EM} the electromechanical force. The different force components can be further written as

$$F_0 = kd_0 \tag{3a}$$

$$F_{ES} = F_{ES}^{Tip} + F_{ES}^{Cant} \tag{3b}$$

$$F_{EM} = F_{EM}^{Piezo} + F_{EM}^{Flexo} \tag{3c}$$

where k is the spring constant of the AFM cantilever and d_0 is the deflection set point, that is, the amount of deflection the cantilever experiences while in constant contact with the sample. The electrostatic force is split into contributions from the tip, F_{ES}^{Tip}, and the cantilever, F_{ES}^{Cant}, and the electromechanical force is split into components from piezoelectricity, F_{EM}^{Piezo}, and flexoelectricity, F_{EM}^{Flexo}.

The elastic contribution comes from the PFM measurement being a contact-mode AFM technique. The AFM tip is brought into contact with the sample surface and a constant feedback loop attempts to keep the tip and cantilever at a constant level of deflection, d_0. The constant deflection will create a constant elastic force given by eq 3a. Because the PFM measurement uses a lock-in amplifier which only amplifies signals at the same frequency as the reference signal, the constant elastic force will have no effect on the PFM signal.

However, during the scanning motion, the feedback system will be moving the tip vertically with the topography of the sample to maintain a constant deflection. This gives rise to two possible concerns: (1) the feedback frequencies may interfere with the applied drive frequency, and (2) the tip motion from changing topography could cause topographic artifacts if motion occurs at the same frequency as V_d. A proper V_d frequency is chosen by taking a frequency sweep of the PR amplitude and choosing a frequency within a range which gives a largely frequency-independent PR amplitude (Supporting Information Note 6 and Figure S7). In this case, 60 kHz was chosen as the V_d frequency. Topographic artifacts from tip motion are ruled out by taking two successive PFM scans, one with V_d applied and one without, as shown in Figures 3 and 5. The voltage-off condition serves as an appropriate background measurement in which any tip motion from topography can be subtracted from the actual PFM signal. Because using the substrate or the voltage-off condition as the background signal gives consistent results, we conclude that the tip motion due to scanning does not have any noticeable effects on the measurement for either substrate.

The next possible contribution to the total force comes from electrostatic forces between the AFM probe and the substrate. These forces can come from the AFM tip or the AFM cantilever, as described by eq 3b. Contributions from the cantilever would act as parallel-plate capacitor-like interactions from the rectangular beam cantilever to the substrate. The dimensions of the cantilever used here are 125 μm × 35 μm, so any electrostatic interactions from the cantilever would be averaged over this entire area. Since Figures 3 and 5 show clear variation with submicron resolution, electrostatic interactions from the cantilever are concluded to be minimal.

Similarly, electrostatic forces from the AFM tip can contribute to the total force. This force can be written as[29]

$$F_{ES}^{Tip} = -\frac{1}{2}\frac{dC_{Tip}}{dz}\left(V_{DC} + V_{AC}\sin(\omega t) + \frac{\Delta\varphi}{q}\right)^2 \tag{4}$$

where C_{Tip}, V_{DC}, V_{AC}, ω, t, $\Delta\varphi$, and q are the tip capacitance, applied DC voltage, applied AC voltage amplitude, frequency, time, work function difference between the tip and area under the tip, and electron charge magnitude, respectively. Because the PFM experiment uses a lock-in amplifier to measure tip deflection, it is sufficient to consider only the first harmonic of eq 4, yielding

$$F_{ES,1\omega}^{Tip} \propto \left(V_{DC} + \frac{\Delta\varphi}{q}\right)V_{AC} \tag{5}$$

This relation provides multiple insights for detecting electrostatic contributions to the PR signal. To determine if electrostatic forces are significant, a DC bias sweep can be performed while measuring the resulting PR amplitude. A linear absolute-value dependence on V_{DC} with a minimum at $V_{DC} = \Delta\varphi/q$ is expected if electrostatic forces are playing a role. Figure S8 shows a piezoresponse amplitude versus V_{DC} sweep at a drive frequency of 60 kHz and V_{AC} = 8 V. The piezoresponse amplitude is independent of V_{DC} under these conditions, indicating that electrostatic effects and any differences between the workfunctions of the two materials are not significant and can be neglected.

With the elimination of the first two terms in eq 2, the PFM signal must be coming from electromechanical effects. The first effect to consider is piezoelectricity, which is what the PFM was originally designed to measure. The piezoelectric tensor for monolayer MoS_2 can be written as[11]

$$d_{ij} = \begin{bmatrix} d_{11} & -d_{11} & 0 & 0 & 0 & 0 \\ 0 & 0 & 0 & 0 & 0 & -2d_{11} \\ 0 & 0 & 0 & 0 & 0 & 0 \end{bmatrix} \tag{6}$$

where the indices correspond to those in the following definition of converse piezoelectricity

$$\varepsilon_j = d_{ij}E_i \tag{7}$$

Here, ε_j is the strain tensor employing Voigt notation and E_i is the electric field. It is important to note that the piezoelectric tensor for MoS_2 has nonzero components only within the plane of its atoms and has zero components for all out-of-plane responses. This indicates that there should be no piezoelectric effect out-of-plane. However, our experiments yield a nonzero

DOI: 10.1021/acs.nanolett.7b02123
Nano Lett. 2017, 17, 5464−5471

value for d_{33}^{eff}, suggesting that this signal could be originating from the flexoelectric effect instead of the piezoelectric effect.

The converse flexoelectric tensor for MoS_2 is given by[24]

$$\mu_{mn}^{*} = \begin{bmatrix} \mu_{11}^{*} & 0 & 0 & 0 & \mu_{15}^{*} & 0 & 0 & 0 & \mu_{19}^{*} \\ \mu_{11}^{*} & 0 & 0 & 0 & \mu_{11}^{*} & 0 & 0 & 0 & \mu_{19}^{*} \\ \mu_{31}^{*} & 0 & 0 & 0 & \mu_{31}^{*} & 0 & 0 & 0 & \mu_{39}^{*} \\ 0 & 0 & 0 & 0 & 0 & \mu_{46}^{*} & 0 & \mu_{48}^{*} & 0 \\ 0 & 0 & \mu_{46}^{*} & 0 & 0 & 0 & \mu_{48}^{*} & 0 & 0 \\ 0 & \mu_{11}^{*} - \mu_{15}^{*} & 0 & \mu_{11}^{*} - \mu_{15}^{*} & 0 & 0 & 0 & 0 & 0 \end{bmatrix} \tag{8}$$

where the * indicates that the converse representation is being used and the indices are defined using the converse flexoelectric equation

$$\sigma_{ij} = \mu_{ijkl}^{*} \frac{\partial E_k}{\partial x_l} \tag{9}$$

where σ_{ij} is the stress tensor. The four indices can be transformed to two by using Voigt notation for ij, while kl follow 11 → 1, 12 → 2, 13 →3, 21 → 4, 22 → 5, 23 → 6, 31 → 7, 32 → 8, 33 → 9 to yield μ_{mn}^{*}.[24]

To a good approximation, we can assume that the electric field in the MoS_2 layer is perpendicular to the surface of the Au and thus the plane of the MoS_2 atoms. With this assumption, the contribution of the first six columns of eq 8 to the electromechanical response of MoS_2 can be neglected. Also, the first two rows describe stresses created in-plane, which will not influence the PFM measurement. Possible contributions to an out-of-plane electromechanical response from an out-of-plane electric field then include μ_{39}^{*} and μ_{48}^{*}. The former is an out-of-plane stress caused by a vertical electric field changing through the thickness of the MoS_2. The latter is an out-of-plane shear-stress mode caused by a vertical electric field varying laterally as it spreads away from the AFM tip.

In general, a superposition of both μ_{39}^{*} and μ_{48}^{*} will contribute to a measurable d_{33}^{eff} value. Although the electromechanical response can be thought of as an effective piezoelectric response, in light of the above analysis it may be more appropriate to refer to the value in this case as an effective flexoelectric response, μ_{eff}^{*}.

To obtain a rough estimate of μ_{eff}^{*} from the measured d_{33}^{eff}, the gradient $\partial E_3/\partial x_3$ is assumed to dominate and is estimated to be $2V_d/t^2$ (see Supporting Information Note 7 for details). These assumptions combined with eq 9, and $\sigma = Y\varepsilon$ where Y is Young's modulus, yield the equation

$$\mu_{\text{eff}}^{*} = \frac{\Delta z}{V_d} \cdot Y \cdot \frac{t}{2} = d_{33}^{\text{eff}} \cdot Y \cdot \frac{t}{2} \tag{10}$$

where Δz is the vertical deflection of the MoS_2. By taking Y = 270 GPa[37] and t to be a monolayer thickness of 6.5 Å,[38] our PFM measurements for MoS_2 on Au and Al_2O_3/Si yield values for μ_{eff}^{*} of 0.08 and 0.12 nC/m, respectively. These estimates are calculated from measurements only on monolayer MoS_2 and further work is needed to analyze how the flexoelectric response would respond with increasing thickness of MoS_2 (see Supporting Information Note 8).

Previous studies[15] have reported that perovskite ceramics in the paraelectric phase have a μ_{eff} on the order of 1−100 μC/m while single crystal perovskites are on the order of 1 nC/m. Values of μ_{mn} for different measurement techniques and those obtained via experiment versus theory can also vary by orders-of-magnitude but are slowly converging.

A common way to get an order of magnitude estimate of the flexoelectric coefficient of a material is to use an estimate developed by Kogan.[39] He estimates the flexocoupling coefficient with the equation

$$f \approx \frac{q}{4\pi\epsilon_0 a} \tag{11}$$

where a is the lattice constant of the material. With the definition

$$\mu \equiv \chi f \tag{12}$$

where χ is the susceptibility of MoS_2, an order of magnitude estimate of μ_{eff} can be obtained for MoS_2. Taking a = 3.2 Å[40] and χ to be $3\epsilon_0$,[41] the estimate of μ_{eff} is 0.12 nC/m. This is remarkably similar to the values derived from our experiments above.

The possibility of contamination on MoS_2 causing the measured out-of-plane electromechanical effects should not be overlooked. X-ray photoelectron spectroscopy (XPS) has been performed to detect the presence of various elements on the sample surfaces. Excess carbon, oxygen, and silicon are seen on the surface of the samples (see Supporting Information Note 9 and Table S1). Much of this is likely to be residue remaining on the surfaces after the polydimethylsiloxane (PDMS) transfer process, adventitious carbon that coats most surfaces when exposed to air, potentially other hydrocarbons, or unreacted MoO_3 precursor from the CVD process. The residue blankets the surface as it is detectable on the Au surface which contacts the PDMS but does not contain MoS_2. The substrate with residue gives little PFM signal, and the background subtraction process should remove most of the contribution to the signal generated from the residue. This does not conclusively rule out that the residue interacts differently with the MoS_2 than the substrate or that the slightly higher oxygen content on the sample affects the measurement. Further analysis is needed to definitively rule out contaminations affecting the measurement. However, the current experiment and analysis yields a strong possibility that out-of-plane flexoelectricity is present in monolayer MoS_2.

In summary, this work has shown that monolayer MoS_2 has an average measurable out-of-plane electromechanical response with a d_{33}^{eff} of 1.03 ± 0.22 pm/V on Au and 1.35 ± 0.24 pm/V on Al_2O_3/Si. There is strong evidence that its origin is from the flexoelectric effect rather than the piezoelectric effect, and an estimate of the effective flexoelectric coefficient μ_{eff}^{*} yields 0.10 nC/m. The presence of flexoelectricity in 2D materials has implications across many fields. In 2D material electronics, for example, roughness in the substrate surface could create local curvature and thus local polarization that could affect electronic device performance.[42] It also opens the door to making new types of nanoscale sensors, actuators, or energy harvesters which could be used in conjunction with piezoelectricity to enhance operation.

Methods. Monolayer MoS_2 is grown via CVD on SiO_2 from solid precursors.[43] The as-grown MoS_2 is under roughly 0.21% residual tensile strain,[44] which is released during the transfer process. A PDMS stamp and a water bath are used to separate the MoS_2 from the growth substrate. The PDMS/MoS_2 is then placed on the receiving substrate, Au/Si or Al_2O_3/Si, and

DOI: 10.1021/acs.nanolett.7b02123
Nano Lett. 2017, 17, 5464−5471

heated with a hot plate to 50 °C. Slowly peeling away the PDMS transfers the MoS_2 to the substrate (see Figure S2 for details).

The Au sample is created via electron beam evaporation onto an n^{++} silicon substrate. A 5 nm titanium adhesion layer is first deposited followed by 70 nm of Au. The Al_2O_3/Si sample is fabricated by first submerging a n^{++} doped silicon substrate in 80:1 diluted HF to remove any oxide layer. The bare silicon is then immediately transferred into a Fiji ALD system. Using a trimethylaluminum precursor, a 5.3 nm thick layer of Al_2O_3 is deposited and thickness measured with a J.A. Woollam M-2000 DI ellipsometer.

Raman and PL data are taken using a Renishaw inVia Raman microscope with a 532 nm laser. PL and Raman data of the MoS_2 taken on the growth substrate, PDMS stamp, and Au sample show a clear relaxation of strain after the MoS_2 is removed from the growth substrate (see Figure S6).

PFM measurements are done on a Bruker (formerly Veeco) Dimension Icon AFM. Conductive cobalt−chromium AFM cantilevers are used (Bruker MESP-RC-V2) for PFM measurements. Tapping mode AFM images were taken using etched silicon cantilevers (Bruker TESP). A PFM drive frequency of 60 kHz and a drive amplitude of 8 V is used in all PFM measurements. See Supporting Information for more details.

■ ASSOCIATED CONTENT

Supporting Information

(PDF) The Supporting Information is available free of charge on the ACS Publications website at DOI: 10.1021/acs.nanolett.7b02123.

PFM setup, equation for d_{33}^{eff} from raw PFM Data, CVD-grown MoS_2 transfer process, MoS_2 thickness determination and optical characterization difficult, MoS_2 on Au thickness determination, MoS_2 on Al_2O_3 thickness determination, MoS_2 on SiO_2 growth substrate thickness determination, photoluminescence measurements, background subtraction for d_{33}^{eff} estimation, uncertainty estimation, voltage drop through MoS_2 on Al_2O_3, determination of drive frequency for PFM, piezoresponse amplitude vs DC bias sweep, estimating μ_{eff}^{*}, electromechanical response with increasing MoS_2thickness, XPS measurements (PDF)

■ AUTHOR INFORMATION

Corresponding Authors

*E-mail: ety@ece.utexas.edu. Phone: 512-232-5167 (E.T.Y.).
*E-mail: nanshulu@utexas.edu. Phone: 512-471-4208 (N.L.).

ORCID

Christopher J. Brennan: 0000-0001-8523-2895

Author Contributions

C.J.B. performed the sample fabrication, AFM, PFM, Raman, photoluminescence, and data analysis. R.G. and S.B. provided CVD grown MoS_2 and assisted in the transfer process. K.K. assisted in AFM measurements. N.L. and E.T.Y. assisted in project design and supervised research. C.J.B., N.L., and E.T.Y. wrote the manuscript.

Notes

The authors declare no competing financial interest.

■ ACKNOWLEDGMENTS

This work was supported by the NSF CMMI Award under Grant 1351875, NSF DMR Award under Grant 1311866, and was performed in part at the University of Texas Microelectronics Research Center, a member of the National Nanotechnology Coordinated Infrastructure (NNCI), which is supported by the National Science Foundation (Grant ECCS-1542159). E.T.Y. acknowledges the Judson S. Swearingen Regents Chair in Engineering at the University of Texas at Austin. S.K.B. acknowledges the U.S. Army Small Business Innovation Research (SBIR) Program office and the U.S. Army Research Office under Contract No. W911NF-16-C-0032. C.J.B. acknowledges Dr. Brooks Carlton Fowler Endowed Presidential Graduate Fellowship in Electrical and Computer Engineering and the Temple Foundation Graduate Microelectronic and Computer Development Fellowship in Engineering of UT-Austin. The authors acknowledge Dr. Hugo Celio for assistance in XPS measurements and Liu Wang for discussions on the calculations.

■ ABBREVIATIONS

AFM, atomic force microscopy; CVD, chemical vapor deposition; MEMS, microelectromechanical systems; PDMS, polydimethylsiloxane; PFM, piezoresponse force microscopy; PL, photoluminescence; PR, piezoresponse; TMDs, transition metal dichalcogenides; XPS, X-ray photoelectron spectroscopy

■ REFERENCES

(1) Fischetti, M. V.; Laux, S. E. *J. Appl. Phys.* **1996**, *80*, 2234−2252.
(2) Hill, E. W.; Vijayaragahvan, A.; Novoselov, K. *IEEE Sens. J.* **2011**, *11*, 3161−3170.
(3) Wang, Q. M.; Du, X. H.; Xu, B.; Cross, L. E. *IEEE Trans. Ultrason. Ferroelectr. Freq. Control* **1999**, *46*, 638−646.
(4) Xu, S.; Qin, Y.; Xu, C.; Wei, Y.; Yang, R.; Wang, Z. L. *Nat. Nanotechnol.* **2010**, *5*, 366−373.
(5) Radisavljevic, B.; Radenovic, A.; Brivio, J.; Giacometti, V.; Kis, A. *Nat. Nanotechnol.* **2011**, *6*, 147−150.
(6) Nair, R. R.; Blake, P.; Grigorenko, A. N.; Novoselov, K. S.; Booth, T. J.; Stauber, T.; Peres, N. M. R.; Geim, A. K. *Science* **2008**, *320*, 1308.
(7) Lee, G.-H.; Yu, Y.-J.; Cui, X.; Petrone, N.; Lee, C.-H.; Choi, M. S.; Lee, D.-Y.; Lee, C.; Yoo, W. J.; Watanabe, K.; Taniguchi, T.; Nuckolls, C.; Kim, P.; Hone, J. *ACS Nano* **2013**, *7*, 7931−7936.
(8) Kim, K. S. K. S.; Zhao, Y.; Jang, H.; Lee, S. Y.; Kim, J. M.; Kim, K. S. K. S.; Ahn, J.-H.; Kim, P.; Choi, J.-Y.; Hong, B. H. *Nature* **2009**, *457*, 706−710.
(9) Wu, W.; Wang, L.; Li, Y.; Zhang, F.; Lin, L.; Niu, S.; Chenet, D.; Zhang, X.; Hao, Y.; Heinz, T. F.; Hone, J.; Wang, Z. L. *Nature* **2014**, *514*, 470−474.
(10) Qi, J.; Lan, Y.-W.; Stieg, A. Z.; Chen, J.-H.; Zhong, Y.-L.; Li, L.-J.; Chen, C.-D.; Zhang, Y.; Wang, K. L. *Nat. Commun.* **2015**, *6*, 7430.
(11) Duerloo, K. A. N.; Ong, M. T.; Reed, E. J. *J. Phys. Chem. Lett.* **2012**, *3*, 2871−2876.
(12) Kim, S. K.; Bhatia, R.; Kim, T.-H.; Seol, D.; Kim, J. H.; Kim, H.; Seung, W.; Kim, Y.; Lee, Y. H.; Kim, S.-W. *Nano Energy* **2016**, *22*, 483−489.
(13) Zhu, H.; Wang, Y.; Xiao, J.; Liu, M.; Xiong, S.; Wong, Z. J.; Ye, Z.; Ye, Y.; Yin, X.; Zhang, X. *Nat. Nanotechnol.* **2014**, *10*, 151−155.
(14) Yudin, P. V.; Tagantsev, a K. *Nanotechnology* **2013**, *24*, 432001.
(15) Zubko, P.; Catalan, G.; Tagantsev, A. K. *Annu. Rev. Mater. Res.* **2013**, *43*, 387−421.
(16) Nguyen, T. D.; Mao, S.; Yeh, Y.-W.; Purohit, P. K.; McAlpine, M. C. *Adv. Mater.* **2013**, *25*, 946−974.
(17) Ahmadpoor, F.; Sharma, P. *Nanoscale* **2015**, *7*, 16555−16570.
(18) Akinwande, D.; Brennan, C. J.; Bunch, J. S.; Egberts, P.; Felts, J. R.; Gao, H.; Huang, R.; Kim, J.; Li, T.; Li, Y.; Liechti, K. M.; Lu, N.;

DOI: 10.1021/acs.nanolett.7b02123
Nano Lett. 2017, 17, 5464−5471

Park, H. S.; Reed, E. J.; Wang, P.; Yakobson, B. I.; Zhang, T.; Zhang, Y.-W.; Zhou, Y.; Zhu, Y. *Extrem. Mech. Lett.* **2017**, *13*, 42−77.
(19) Dumitrică, T.; Landis, C. M.; Yakobson, B. I. *Chem. Phys. Lett.* **2002**, *360*, 182−188.
(20) Kalinin, S. V.; Meunier, V. *Phys. Rev. B: Condens. Matter Mater. Phys.* **2008**, *77*, 1−4.
(21) Kvashnin, A. G.; Sorokin, P. B.; Yakobson, B. I. *J. Phys. Chem. Lett.* **2015**, *6*, 2740−2744.
(22) Naumov, I.; Bratkovsky, A. M.; Ranjan, V. *Phys. Rev. Lett.* **2009**, *102*, 2−5.
(23) Duerloo, K.-A. N.; Reed, E. J. *Nano Lett.* **2013**, *13*, 1681−1686.
(24) Shu, L.; Wei, X.; Pang, T.; Yao, X.; Wang, C. *J. Appl. Phys.* **2011**, *110*, 104106.
(25) Zelisko, M.; Hanlumyuang, Y.; Yang, S.; Liu, Y.; Lei, C.; Li, J.; Ajayan, P. M.; Sharma, P. *Nat. Commun.* **2014**, *5*, 4284.
(26) da Cunha Rodrigues, G.; Zelenovskiy, P.; Romanyuk, K.; Luchkin, S.; Kopelevich, Y.; Kholkin, A. *Nat. Commun.* **2015**, *6*, 7572.
(27) Jungk, T.; Hoffmann, Á.; Soergel, E. *Appl. Phys. Lett.* **2007**, *91*, 253511.
(28) Jungk, T.; Hoffmann, Á.; Soergel, E. *Appl. Phys. A: Mater. Sci. Process.* **2007**, *86*, 353−355.
(29) Kalinin, S.; Bonnell, D. *Phys. Rev. B: Condens. Matter Mater. Phys.* **2002**, *65*, 125408.
(30) Yang, S. M.; Mazet, L.; Okatan, M. B.; Jesse, S.; Niu, G.; Schroeder, T.; Schamm-Chardon, S.; Dubourdieu, C.; Baddorf, A. P.; Kalinin, S. V. *Appl. Phys. Lett.* **2016**, *108*, 252902.
(31) Labuda, A.; Proksch, R. *Appl. Phys. Lett.* **2015**, *106*, 253103.
(32) Proksch, R. *J. Appl. Phys.* **2015**, *118*, 072011.
(33) Jungk, T.; Hoffmann, Á.; Soergel, E. *J. Microsc.* **2007**, *227*, 72−78.
(34) Jungk, T.; Hoffmann, A.; Soergel, E. *Appl. Phys. Lett.* **2006**, *89*, 163507.
(35) Buscema, M.; Steele, G. A.; van der Zant, H. S. J.; Castellanos-Gomez, A. *Nano Res.* **2014**, *7*, 561.
(36) Lee, C.; Yan, H.; Brus, L. E.; Heinz, T. F.; Hone, J.; Ryu, S. *ACS Nano* **2010**, *4*, 2695−2700.
(37) Bertolazzi, S.; Brivio, J.; Kis, A. *ACS Nano* **2011**, *5*, 9703−9709.
(38) Novoselov, K. S.; Jiang, D.; Schedin, F.; Booth, T. J.; Khotkevich, V. V.; Morozov, S. V.; Geim, A. K. *Proc. Natl. Acad. Sci. U. S. A.* **2005**, *102*, 10451−10453.
(39) Kogan, S. M.; et al. *Sov. Phys. Solid State* **1964**, *5*, 2069−70.
(40) Ganatra, R.; Zhang, Q. *ACS Nano* **2014**, *8*, 4074−4099.
(41) Santos, E. J. G.; Kaxiras, E. *ACS Nano* **2013**, *7*, 10741−10746.
(42) Shin, B. G.; Han, G. H.; Yun, S. J.; Oh, H. M.; Bae, J. J.; Song, Y. J.; Park, C.; Lee, Y. H. *Adv. Mater.* **2016**, *28*, 9378−9384.
(43) Liu, Y.; Ghosh, R.; Wu, D.; Ismach, A.; Ruoff, R.; Lai, K. *Nano Lett.* **2014**, *14*, 4682−4686.
(44) Lloyd, D.; Liu, X.; Christopher, J. W.; Cantley, L.; Wadehra, A.; Kim, B. L.; Goldberg, B. B.; Swan, A. K.; Bunch, J. S. *Nano Lett.* **2016**, *16*, 5836−5841.

DOI: 10.1021/acs.nanolett.7b02123
Nano Lett. 2017, 17, 5464−5471